
Estimating the Unique Information of Continuous Variables

Ari Pakman Columbia University **Amin Nejatbakhsh** Columbia University **Dar Gilboa** Harvard University **Abdullah Makkeh** Georg August University

Luca Mazzucato University of Oregon **Michael Wibral** Georg August University **Elad Schneidman** Weizmann Institute

Abstract

The integration and transfer of information from multiple sources to multiple targets is a core motive of neural systems. The emerging field of partial information decomposition (PID) provides a novel information-theoretic lens into these mechanisms by identifying synergistic, redundant, and unique contributions to the mutual information between one and several variables. While many works have studied aspects of PID for Gaussian and discrete distributions, the case of general continuous distributions is still uncharted territory. In this work we present a method for estimating the unique information in continuous distributions, for the case of one versus two variables. Our method solves the associated optimization problem over the space of distributions with fixed bivariate marginals by combining copula decompositions and techniques developed to optimize variational autoencoders. We obtain excellent agreement with known analytic results for Gaussians, and illustrate the power of our new approach in several brain-inspired neural models. Our method is capable of recovering the effective connectivity of a chaotic network of rate neurons, and uncovers a complex trade-off between redundancy, synergy and unique information in recurrent networks trained to solve a generalized XOR task.

1 Introduction and background

In neural systems, often multiple neurons are driven by one external event or stimulus; conversely multiple neural inputs can converge onto a single neuron. A natural question in both cases is how multiple variables hold information about the singleton variable. In their seminal work [1], Williams and Beer proposed an axiomatic extension of classic information theory to decompose the mutual information between multiple source variables and a single target variable in a meaningful way. For the case of two sources X_1, X_2 , their partial information decomposition (PID) amounts to expressing the mutual information of X_1, X_2 with a target Y as a sum of four non-negative terms,

$$I(Y : (X_1, X_2)) = U(Y : X_1 \setminus X_2) + U(Y : X_2 \setminus X_1) + R(Y : (X_1, X_2)) + S(Y : (X_1, X_2)), \quad (1.1)$$

corresponding to unique (U_1, U_2), redundant (R) and synergistic (S) contributions, respectively. These terms should also obey the consistency equations

$$I(Y : X_1) = R(Y : (X_1, X_2)) + U(Y : X_1 \setminus X_2), \quad (1.2)$$

$$I(Y : X_2) = R(Y : (X_1, X_2)) + U(Y : X_2 \setminus X_1). \quad (1.3)$$

The PID has proved useful in understanding information processing by distributed systems in a diverse array of fields including machine learning [2, 3], earth science [4] and cellular automata [5],

and particularly in neuroscience [6–10], where notions of synergy and redundancy, traditionally considered mutually exclusive and distinguished by the sign of

$$\begin{aligned}\Delta &= I(Y : (X_1, X_2)) - I(Y : X_1) - I(Y : X_2), \\ &= S(Y : (X_1, X_2)) - R(Y : (X_1, X_2)),\end{aligned}\tag{1.4}$$

have long played a central role in the quest to understand how neural circuits integrate information from multiple sources [11–14]. The novelty of the PID framework here is in separating the measures of synergy and redundancy in (1.4).

The above abstract formulation of PID provides three equations for four unknowns, and only becomes operational once one of U_1 , U_2 , R , or S is defined. This has been done in [15] via a definition of the unique information:

Definition 1 (BROJA [15]). *Given three random variables (Y, X_1, X_2) with joint probability density $p(y, x_1, x_2)$, the unique information U_1 of X_1 with respect to Y is*

$$U(Y : X_1 \setminus X_2) = \min_{q \in Q} I_q(Y : X_1 | X_2),\tag{1.5}$$

$$= \min_{q \in Q} \int dy dx_1 dx_2 q(y, x_1, x_2) \log \left(\frac{q(y, x_1 | x_2)}{q(y | x_2) q(x_1 | x_2)} \right),\tag{1.6}$$

where

$$Q = \{q(y, x_1, x_2) \mid q(y, x_i) = p(y, x_i), i = 1, 2\}.\tag{1.7}$$

In words, we minimize the conditional mutual information $I(Y : X_1 | X_2)$ over the space of density functions that preserve the marginal densities $p(y, x_1)$ and $p(y, x_2)$. The above definition implies, along with (1.2)-(1.3), that the unique and redundant information only depend on the marginals $p(y, x_1)$, $p(y, x_2)$, and that the synergy can only be estimated from the full $p(y, x_1, x_2)$.

The original definition in [15] was limited to discrete random variables. Here, we show that the extension to continuous variables is well-defined and can be practically estimated.

Motivation from decision theory [15]. Consider for simplicity discrete variables. A decision maker DM_1 can choose an action a from a finite set \mathcal{A} , and receives a reward $u(a, y)$ based on the selected action and the state y , which occurs with probability $p(y)$. Notably, DM_1 has no knowledge of y , but observes instead a random signal x_1 sampled from $p(x_1 | y)$. Choosing the action maximizing the expected reward for each x_1 , his maximal expected reward is

$$R_1 = \sum_{x_1} p(x_1) \max_{a | x_1} \sum_y p(y | x_1) u(a, y).\tag{1.8}$$

DM_1 is said to have no unique information about y w.r.t. another decision maker DM_2 that observes $x_2 \sim p(x_2 | y)$ – if $R_2 \geq R_1$ for any set \mathcal{A} , any distribution $p(y)$, and any reward function $u(a, y)$. A celebrated theorem by Blackwell [16, 17] states that such a generic advantage by DM_2 occurs iff there exist a stochastic matrix $q(x_1 | x_2)$ which satisfies

$$p(x_1 | y) = \sum_{x_2} p(x_2 | y) q(x_1 | x_2).\tag{1.9}$$

But this occurs precisely when the unique information (1.5) vanishes, since then there exists a joint distribution $q(y, x_1, x_2)$ in Q for which $y \perp x_1 | x_2$, which implies $q(x_1 | x_2, y) = q(x_1 | x_2)$, and thus (1.9) holds. Similar results exist for continuous variables [18, 19]. Thus the unique information from Definition 1 quantifies a departure from Blackwell’s relation (1.9).

In this work we present a definition and a method to estimate the BROJA unique information for generic continuous probability densities. Our approach is based on the observation that the constraints (1.7) can be satisfied with an appropriate copula parametrization, and makes use of techniques developed to optimize variational autoencoders. We only consider one-dimensional Y, X_1, X_2 for simplicity, but the method can be naturally extended to higher dimensional cases. In Section 2 we review related works, in Section 3 we present our method and Section 4 contains several illustrative examples.

2 Related works

Partial information decomposition offers a solution to a repeated question that was not addressed by ‘classical’ information theory regarding the relations between two sources and a target [1]. From a mathematical perspective a ‘functional definition’ has to be made, meaning that such a definition should align with our intuitive notions. Yet, as shown in [20], not all intuitively desirable properties of a PID can be realized simultaneously. Thus, different desirable properties are chosen for distinct application scenarios. Thus, various proposals for decomposition measures are not seen as conflicting but as having different operational interpretations. For example, the BROJA approach used here builds on desiderata from decision theory, while other approaches appeal to game theory [21] or the framework of Kelly gambling [22]. Yet other approaches use arguments from information geometry [23]. Other approaches assume agents receiving potentially conflicting or incomplete information about the source variables for the purpose of inference or decryption (see e.g. [24, 25]). In [26] the authors separate the specific operational interpretations of PID measures from the general structure of information decomposition.

The actual computation of the BROJA unique information is non-trivial, even for discrete variables. Optimization methods exist for the latter case [27–29], and analytic solutions are only known when all the variables are univariate binary [30]. For continuous probability densities, an earlier definition aligned with the BROJA measure was made by Barret [31], but only applies to Gaussian variables. For Barret’s measure, an analytic solution is known when $p(y, x_1, x_2)$ is a three-dimensional Gaussian density [31], but does not generalize to higher dimensional Gaussians [32].

3 Bounding and estimating the unique information

We proceed in two steps. We first introduce a parametrization of the optimization space Q in (1.7) and then introduce and optimize an upper bound on the unique information.

3.1 Parametrizing the optimization space with copulas

To characterize the optimization space Q in (1.5)-(1.7), it is convenient to recall that according to Sklar’s theorem [33], any n -variate probability density can be expressed as

$$p(x_1 \dots x_n) = p(x_1) \dots p(x_n) c(u_1 \dots u_n), \quad (3.1)$$

where $p(x_i)$ is the marginal and $u_i = F(x_i)$ is the CDF of each variable. The dependency structure among the variables is encoded in the function $c: [0, 1]^n \rightarrow [0, 1]$. This is a *copula* density, a probability density on the unit hypercube with uniform marginals [34],

$$\int_{[0,1]^{n-1}} \prod_{j=1, j \neq i}^n du_j c(u_1 \dots u_n) = 1 \quad \forall i. \quad (3.2)$$

Note that under univariate reparametrizations $z'_i = g(z_i)$, the u_i ’s and the copula c remain invariant. For an overview of copulas in machine learning, see [35].

Proposition 1. *Under the BROJA Definition 1 of unique information, all the terms of the partial information decomposition in (1.1)-(1.3) are independent of the univariate marginals $p(x_1), p(x_2), p(y)$, and only depend on the copula $c(u_y, u_1, u_2)$.*

Proof. Expressing $q(y, x_1, x_2), q(x_1, x_2), q(y, x_2)$ via copula decompositions (3.1), and changing variables as $du_y = q(y)dy$, etc., the objective function in (1.6) becomes

$$I_q(Y : X_1 | X_2) = \int_{[0,1]^3} du_y du_1 du_2 c(u_y, u_1, u_2) \log \left(\frac{c(u_y, u_1, u_2)}{c(u_y, u_2) c(u_1, u_2)} \right). \quad (3.3)$$

Note that the copula of any marginal distribution is the marginal of the copula:

$$c(u_y, u_2) = \int_{[0,1]} du_1 c(u_y, u_1, u_2), \quad c(u_1, u_2) = \int_{[0,1]} du_y c(u_y, u_1, u_2). \quad (3.4)$$

Thus the optimization objective and the unique information are independent of the univariate marginals. A similar result holds for the mutual information terms in the l.h.s. of (1.1)-(1.3).¹ It follows that none of the PID terms in (1.1)-(1.3) depend on the univariate marginals, and therefore all the PID terms are invariant under univariate reparametrizations of (y, x_1, x_2) . \square

In order to parametrize the optimization space Q in (1.7) using copulas, consider the factorization

$$p(y, x_1, x_2) = p(x_1)p(y|x_1)p(x_2|y, x_1). \quad (3.5)$$

Using the copula decomposition (3.1) for $n = 2$, the last two factors in (3.5) can be expressed as

$$p(y|x_1) = \frac{p(y, x_1)}{p(x_1)} = \frac{p(y)p(x_1)c(y, x_1)}{p(x_1)} = c(u_y, u_1)p(y), \quad (3.6)$$

and similarly

$$p(x_2|y, x_1) = \frac{p(x_1, x_2|y)}{p(x_1|y)}, \quad (3.7)$$

$$= c_{1,2|y}(u_{1|y}, u_{2|y})p(x_2|y), \quad (3.8)$$

$$= c_{1,2|y}(u_{1|y}, u_{2|y})c(u_y, x_2)p(x_2), \quad (3.9)$$

where we defined the conditional CDFs,

$$u_{i|y} = F(u_i|u_y) = \frac{\partial C(u_y, u_i)}{\partial u_y} \quad i = 1, 2 \quad (3.10)$$

and $C(u_y, u_i)$ is the CDF of $c(u_y, u_i)$. Note that the function $c_{1,2|y}(u_{1|y}, u_{2|y})$ in (3.8) is not the conditional copula $c(u_1, u_2|u_y)$, but rather the copula of the conditional $p(x_1, x_2|y)$. Using expressions (3.6) and (3.9), the full density (3.5) becomes

$$p(y, x_1, x_2) = p(y)p(x_1)p(x_2)c(u_y, u_1, u_2), \quad (3.11)$$

where

$$c(u_y, u_1, u_2) = c(u_y, u_1) c(u_y, u_2) c_{1,2|y}(u_{1|y}, u_{2|y}). \quad (3.12)$$

This is a simple case of the pair-copula construction of multivariate distributions [38–40], which allows to expand any n -variate copula as a product of (conditional) bivariate copulas.

Proposition 2. *The copula of the conditional, $c_{1,2|y}(\cdot, \cdot)$, parametrizes the space Q in (1.7).*

Proof. Since $q(y, x_i) = p(y, x_i)$ ($i = 1, 2$), the copula factors in

$$p(y, x_i) = p(y)p(x_i) c(u_y, u_i), \quad i = 1, 2 \quad (3.13)$$

are fixed in Q . Therefore, in the copula decomposition (3.12) for $q(y, x_1, x_2) \in Q$, only the last factor can vary in Q . Let us denote by θ the parameters of a generic parametrization for the copula $c_{1,2|y}(u_{1|y}, u_{2|y})$. Since the latter is conditioned on u_y , the parameters can be taken as a function $\theta(u_y)$. It follows that the copula of q necessarily has the form

$$c_\theta(u_y, u_1, u_2) = c(u_y, u_1) c(u_y, u_2) c_{1,2|\theta(u_y)}(u_{1|y}, u_{2|y}), \quad (3.14)$$

and the parameters of the function $\theta(u_y)$ are the optimization variables.² \square

¹The connection between mutual information and copulas was discussed in [36, 37].

²We note that in multivariate pair-copula expansions it is common to assume constant conditioning parameters θ [41], but we do not make such a simplifying assumption.

3.2 Optimizing an upper bound

Inserting now the expression (3.14) into the objective function (3.3) we get

$$I[\theta] = \mathbb{E}_{c_\theta(u_y, u_1, u_2)} \log [c(u_y, u_1)c_{1,2|\theta(u_y)}(u_{1|y}, u_{2|y})] - \mathbb{E}_{c_\theta(u_1, u_2)} \log c_\theta(u_1, u_2), \quad (3.15)$$

which is our objective function and satisfies the marginal constraints (1.7). Note that apart from the optimization parameters θ , it depends on the bivariate copulas $c(u_y, u_1)$ and $c(u_y, u_2)$ which should be estimated from the observed data. Given D observations $\{y^{(i)}, x_1^{(i)}, x_2^{(i)}\}_{i=1}^D$, we map each value to $[0, 1]$ via the empirical CDFs of each coordinate (y, x_1, x_2) . Computing the latter has a $O(D \log D)$ cost from sorting each coordinate and yields a data set $\{u_y^{(i)}, u_1^{(i)}, u_2^{(i)}\}_{i=1}^D$. The latter set is used to estimate copula densities $c(u_y, u_1)$ and $c(u_y, u_2)$ by fitting several parametric and non-parametric copula models [42], and choosing the best pair of models using the AIC criterion.³ From the learned copulas we also get the conditional CDF functions $u_{i|y} = F(u_i|u_y)$ that appear in the arguments of the first term in (3.15).

A variational upper bound. Minimizing (3.15) directly w.r.t. θ is challenging because the second term depends on the copula marginal $c_\theta(u_1, u_2)$ which has no closed form, as it requires integrating (3.14) w.r.t. u_y . We introduce instead an inference distribution $r_\phi(u_y|u_1, u_2)$, with parameters ϕ , that approximates the conditional copula $c_\theta(u_y|u_1, u_2)$, and consider the bound

$$\log c_\theta(u_1, u_2) = \log \int du'_y c_\theta(u'_y, u_1, u_2) \geq \int du'_y r_\phi(u'_y|u_1, u_2) \log \frac{c_\theta(u'_y, u_1, u_2)}{r_\phi(u'_y|u_1, u_2)}, \quad (3.16)$$

which follows from Jensen's inequality and is tight when $r_\phi(u'_y|u_1, u_2) = c_\theta(u'_y|u_1, u_2)$. This expression gives an upper bound on $I_q[\theta]$, which can be minimized jointly w.r.t. (θ, ϕ) .

A disadvantage of the bound (3.16) is that its tightness depends strongly on the expressiveness of the inference distribution $r_\phi(u'_y|u_1, u_2)$. This situation can be improved by considering a multiple-sample generalization proposed by [44],

$$\log c_\theta(u_1, u_2) \geq D_{A,\theta,\phi}(u_1, u_2) \equiv \mathbb{E}_{p(u_y^{(1)} \dots u_y^{(A)})} \log \left[\frac{1}{A} \sum_{a=1}^A \frac{c_\theta(u_y^{(a)}, u_1, u_2)}{r_\phi(u_y^{(a)}|u_1, u_2)} \right], \quad (3.17)$$

where the expectation is w.r.t. A independent samples of $r_\phi(u'_y|u_1, u_2)$. $D_{A,\theta,\phi}(u_1, u_2)$ coincides with the lower bound in (3.16) for $A = 1$ and satisfies [44]

$$D_{A+1,\theta,\phi}(u_1, u_2) \geq D_{A,\theta,\phi}(u_1, u_2), \quad (3.18)$$

$$\lim_{A \rightarrow \infty} D_{A,\theta,\phi}(u_1, u_2) = \log c_\theta(u_1, u_2). \quad (3.19)$$

Thus, even when $r_\phi(u'_y|u_1, u_2) \neq c_\theta(u'_y|u_1, u_2)$, the bound can be made arbitrarily tight for large enough A . Inserting (3.17) in (3.15), we get finally

$$I_q[\theta] \leq B_1[\theta] + B_2[\theta, \phi], \quad (3.20)$$

where

$$B_1[\theta] = \mathbb{E}_{c_\theta(u_y, u_1, u_2)} \log [c(u_y, u_1)c_{1,2|\theta(u_y)}(u_{1|y}, u_{2|y})], \quad (3.21)$$

$$B_2[\theta, \phi] = -\mathbb{E}_{c_\theta(u_1, u_2)} D_{A,\theta,\phi}(u_1, u_2), \quad (3.22)$$

and we minimize the r.h.s. of (3.20) w.r.t. (θ, ϕ) . Low-variance estimates of the gradients to perform the minimization can be obtained with the reparametrization trick [45, 46], as discussed in detail in Appendix A. In our examples below we use for $c_{1,2|\theta(u_y)}$ a bivariate Gaussian copula (reviewed in Appendix B). Such a copula has just one parameter $\theta \in [-1, +1]$, and thus the optimization is done over the space of functions $\theta(u_y): [0, 1] \rightarrow [-1, +1]$, which we parametrize with a two-layer neural network. Similarly, we parametrize $r_\phi(u_y|u_1, u_2)$ with a two-layer neural network. Details of these networks are in Appendix D.

³For this fitting/model selection step, we used the `pyvinecopu1ib` python package [43].

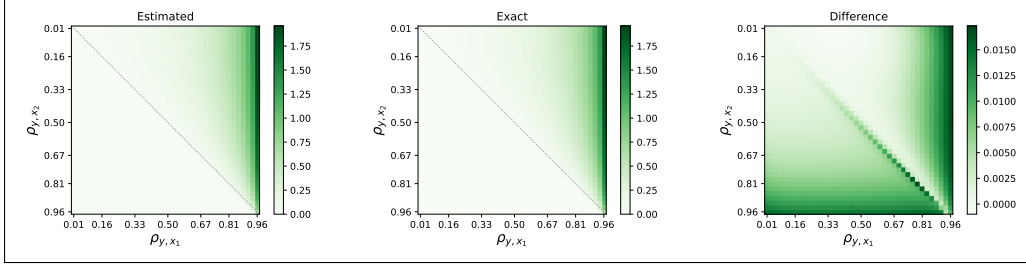


Figure 1: **Estimated vs. exact values of unique information for Gaussians.** For a three-dimensional Gaussian, we show estimates of $U(Y : X_1 \setminus X_2)$ as a function of the correlations ρ_{y,x_i} ($i = 1, 2$), compared with the exact results from [31]. Only for Gaussian distributions are exact results known for continuous variables.

While the term B_2 in our bound is similar to the negative of the ELBO bound in importance weighted autoencoders (IWAEs) [44], there are some differences between the two settings, the most important being that we are interested in the precise value of the bound at the minimum, rather than the learned functions c_θ, r_ϕ . Note also that our latent variables $u_y^{(k)}$ are one-dimensional, as opposed to the usual higher dimensional latent distributions of variational autoencoders, and that the empirical expectation over data observations in IWAEs is replaced in B_2 by the expectation over $c_\theta(u_1, u_2)$, whose parameters are also optimized.

Estimating the other PID terms In the following we adopt the minimal value taken by the upper bound (3.20) as our estimate of U_1 . The other terms in the partial information decomposition are obtained from the consistency relations (1.1)-(1.3), after estimating the mutual informations $I(Y : (X_1, X_2)), I(Y : X_1), I(Y : X_2)$. There are several methods for the latter. In our examples, we use the observed data to fit additional copulas $c(u_1, u_2)$ and $c_{12|\theta(u_y)}$ and estimate $I(Y : X_1) \simeq \frac{1}{D} \sum_{i=1}^D \log c(u_y^{(i)}, u_1^{(i)})$ and similarly for the other terms. Note that all our estimates have sources of potential bias. Firstly, the estimation of the parametric copulas is subject to model or parameter misspecification, which can be ameliorated by more refined model selection strategies. Secondly, the optimized bound might not saturate, biasing the estimate upwards. This can be improved using higher A values and improving the gradient-based optimizer used.

4 Examples

Comparison with exact results for Gaussians. Consider a three-dimensional Gaussian with correlations ρ_{y,x_i} between y, x_i for $i = 1, 2$. The exact solution to (1.5) in this case is [31]

$$U(Y : X_1 \setminus X_2) = \frac{1}{2} \log \left(\frac{1 - \rho_{y,x_2}^2}{1 - \rho_{y,x_1}^2} \right) \mathbb{1}[\rho_{y,x_2} < \rho_{y,x_1}]. \quad (4.1)$$

Fig. 1 compares the above expression with estimates from our method. Here we know that $c_{y,1}$ and $c_{y,2}$ are Gaussian copulas, with parameters $\rho_{y,x_1}, \rho_{y,x_2}$, and we assumed a Gaussian copula for $c_{1,2|y,\theta}(u_{1|y}, u_{2|y})$ as well. For each pair of values $\rho_{y,x_1}, \rho_{y,x_2}$. In this and the rest of the experiments, we optimized the parameters (θ, ϕ) using the ADAM algorithm [47] with a fixed learning rate 10^{-2} during 1200 iterations, and using $A = 50$. The results reported correspond to the mean of the bound in the last 100 iterations. The comparison in Fig. 1 shows excellent agreement.

Model systems of three neurons. The nature of information processing of neural systems is a prominent area of application of the PID framework, since synergy has been proposed as natural measure of information modification [7, 48]. We consider two models:

$$\begin{array}{ll} \text{M1} & \text{M2} \\ (X_1, X_2) \sim \mathcal{N}(0, \rho_{12}^2), & (X_1, X_2) \sim \mathcal{N}(0, \rho_{12}^2), \\ Y = \tanh(w_1 X_1 + w_2 X_2). & Y = X_1^2 / (0.1 + w_1 X_1^2 + w_2 X_2^2). \end{array} \quad (4.2)$$

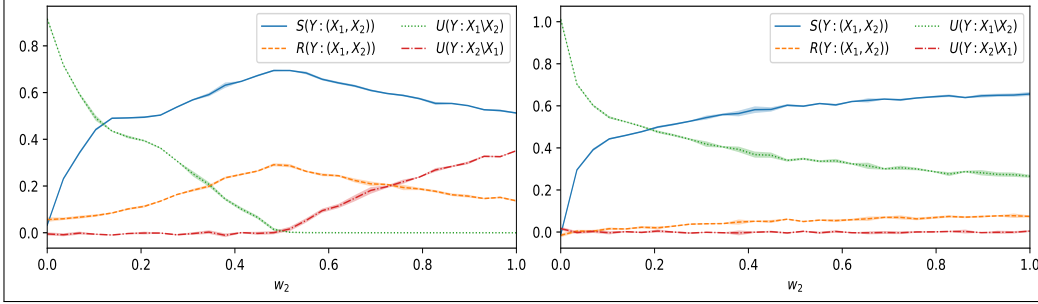


Figure 2: **Partial information decomposition for two neural network models.** In both models (4.2) we fixed $w_1 = 0.5, \rho_{12} = 0.3$, and show the PID terms as a function of the synaptic strength w_2 , normalized by $I(Y : (X_1, X_2))$. We show mean (lines) and standard deviations (shaded area around each line) from 3 runs. *Left:* Model 1: The input of greatest weight conveys all the unique information, and synergy and redundancy both peak as $w_1 = w_2$. *Right:* Model 2: The second input X_2 has negligible unique information contribution, but its synaptic strength w_2 modulates the synergistic term, associated to the modification of information the neuron performs [48].

Both models are parameterized by the correlation ρ_{12} and weights w_1, w_2 . Model 1 is a particularly simple neural network. The tanh activation does not affect its copula, and even for a linear activation function the variables are not jointly Gaussian since Y is deterministic on (X_1, X_2) . Model 2 is inspired by a normalization operation widely believed to be canonical in neural systems [49] and plays a role in common learned image compression methods [50]. The results, presented in Figure 2, are obtained from 3000 samples from each model

Computational aspects of connectivity in recurrent neural circuits. We apply our continuous variable PID to understand computational aspects of the information processing between recurrently coupled neurons (Fig. 3). A large amount of work has been devoted to applying information theoretic measures for quantifying directed pairwise information transfer between nodes in dynamic networks and neural circuits [51]. However, classical information theory only allows for the quantification of information transfer, whereas the framework of PID enables further decomposition of information processing into transfer, storage, and modification, providing further insights into the computation within a recurrent system [52]. Transfer entropy (TE) [53] is a popular measure to estimate the directed transfer of information between pairs of neurons [54, 55], and is sometimes approximated by linear Granger causality. Intuitively, TE between a process X and a process Y measures how much the past of X , X^- , can help to predict the future of Y , Y^+ , accounting for its past Y^- . Although TE quantifies how much information is transferred between neurons, it does not shed light on the computation emerging from the interaction of X^- and Y^- . Simply put, the information transferred from X^- could enter Y^+ , independently of the past state Y^- , or it could be fused in a non-trivial way with the information in the state in Y^- [52, 56]. PID decomposes the TE into **modified transfer** (quantified by $S(Y^+ : X^-, Y^-)$) and **unique transfer** (quantified by $U(Y^+ : X^- \setminus Y^-)$) terms (see the Appendix for a proof):

$$TE(X \rightarrow Y) = I(Y^+ : X^- | Y^-) = U(Y^+ : X^- \setminus Y^-) + S(Y^+ : X^-, Y^-).$$

Furthermore, the information kept by the system through time can be quantified by the **unique storage** (given by $U(Y^+ : Y^- \setminus X^-)$) and **redundant storage** (given by $R(Y^+ : X^-, Y^-)$) in PID [48]. This perspective is a new step towards understanding how the information is processed in recurrent systems beyond merely detecting the direction functional interactions estimated by traditional TE methods (see Appendix G, for details). To explore these ideas, we simulated chaotic networks of rate neurons with an a-priori causal structure consisting of two sub-networks \mathbf{X} and \mathbf{Y} (Fig. 3a, see [57] for more details on causal analyses of this network model). The sub-network \mathbf{X} is a Rossler attractor of three neurons obeying the dynamical equations:

$$\begin{cases} \dot{X}_1 = -X_2 - X_3 \\ \dot{X}_2 = X_1 + \alpha X_2 \\ \dot{X}_3 = \beta + X_3(X_1 - \gamma) \end{cases} \quad (4.3)$$

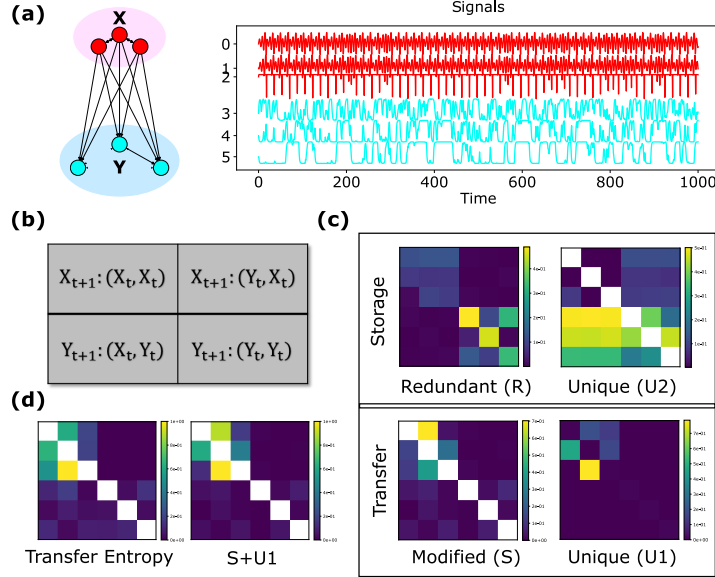


Figure 3: **PID uncovers the effective connectivity and allows for the quantification of storage, modification, and transfer of information in a chaotic network of rate neurons.** **a:** Schematics of recurrent network architecture (left) and representative activity (right). **b:** Schematic of the PID triplets for each 3×3 block of the matrices in c, d. **c:** PID decomposition into modified transfer S , unique transfer U_1 , redundant storage R , and unique storage U_2 for the rate network. The future of X neurons only depends on unique information in the past of X neurons and their synergistic interactions. The interactions between the X and Y sub-networks only contain synergistic information regarding the future of Y but no redundant information; the latter is only present in the interactions confined within each sub-network. **d:** The transfer entropy (TE), estimated via IDTx1 [58], recovers the sum of modified and unique transfer terms $S + U_1$.

where $\{\alpha, \beta, \gamma\} = \{0.2, 0.2, 5.7\}$. There are 100 neurons in the sub-network \mathbf{Y} from which we chose the first three, $Y_{1:3}$, to simulate the effect of unobserved nodes. Neurons within the sub-network Y obey the dynamical equations

$$\dot{Y} = -\lambda Y + 10 \tanh(J_{YX}X + J_{YY}Y) \quad (4.4)$$

where $J_{YX} \in \mathbb{R}^{100 \times 3}$ has all its entries equal to 0.1, and J_{YY} is the recurrent weight matrix of the Y sub-network, sampled as zero-mean, independent Gaussian variables with standard deviation $g = 4$. No projections exist from the downstream sub-network \mathbf{Y} to the upstream sub-network \mathbf{X} . We simulated time series from this network (exhibiting chaotic dynamics, see Fig. 3a) and estimated the PID as unique, redundant, and synergistic contribution of neuron i and neuron j at time t in shaping the future of neuron j at time $t + 1$. For each pair of neurons $Z_i, Z_j \in \{X_{1:3}, Y_{1:3}\}$ we treated $(Z_i^t, Z_j^t, Z_j^{t+1})_{t=1}^T$ as iid samples⁴ and ran PID on these triplets (i, j represent rows and columns in Fig. 3b-d). The PID uncovered the functional architecture of the network and further revealed non-trivial interactions between neurons belonging to the different sub-networks, encoded in four matrices: modified transfer S , unique transfer U_1 , redundant storage R , and unique storage U_2 (details in Fig. 3d). The sum of the modified and unique transfer terms was found to be consistent with the TE (Fig. 3c, TE equal to $S + U_1$, up to estimation bias). The TE itself captured the network effective connectivity, consistent with previous results [55, 57].

Uncovering a plurality of computational strategies in RNNs trained to solve complex tasks. A fundamental goal in neuroscience is to understand the computational mechanisms emerging from

⁴Note that the estimation of the PID from many samples of the triplets $(Z_i^t, Z_j^t, Z_j^{t+1})$ is operationally the same whether such triplets are iid or, as in our case, temporally correlated. This is similar to estimating expectations w.r.t. the equilibrium distribution of a Markov chain by using temporally correlated successive values of the chain. In both cases, the temporal correlations do not introduce bias in the estimator but can increase the variance.

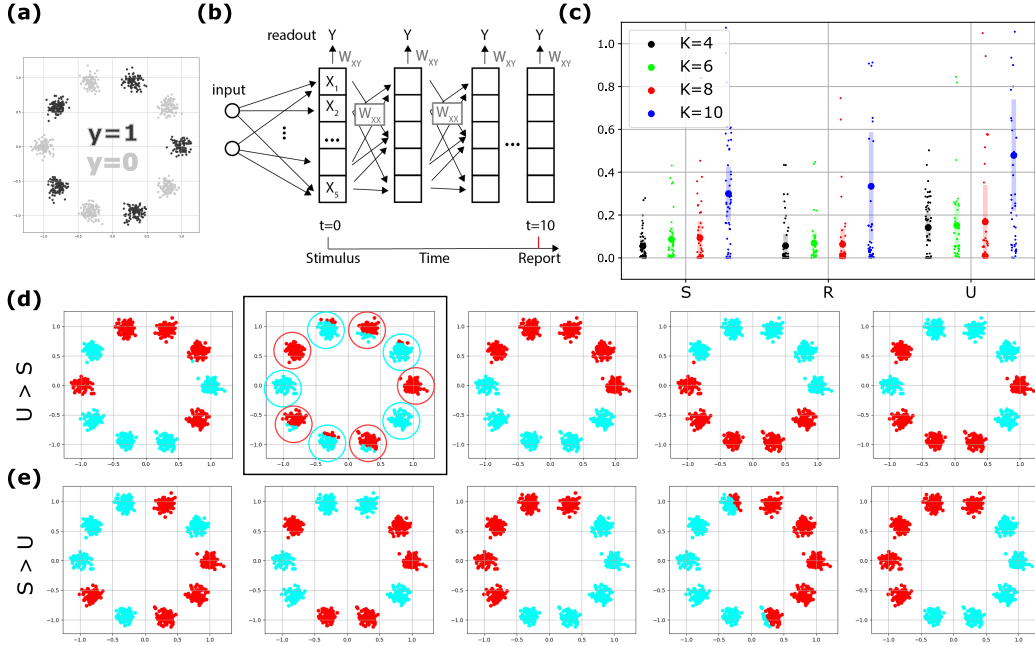


Figure 4: **PID of RNNs trained to solve generalized XOR problem.** **a:** Input data drawn from a 2D Gaussian Mixture Model with K mixture components $X \sim \sum_{k=1}^K \frac{1}{K} \mathcal{N}(X|\mu_k, \sigma I)$ with means lying on the unit circle (grey and black dots represent the two class labels). **b:** Two layer network with 2D input layer, 5 recurrently connected hidden neurons X and one readout neuron Y ; RNN activity unfolds in time (horizontal axis). The input is presented at time $t = 0$, then withdrawn, and the RNN is trained with BPTT to report the decision at $t = 10$. In this representation, layers correspond to time-steps and weights W_{XX} are shared between layers. **c:** PID between output $Y(t)$ and pairs of hidden neurons $X_i(t-1), X_j(t-1)$ for $t = 10$ yielding S, R, U_1, U_2 (distribution over 1000 input samples for each task K ; 20 networks per task). Harder tasks led to an increase in PID measures. **d:** Example receptive fields for a network with $U > S$ shows emergence of grand-mother cells in the hidden layer (red and blue colors represent hidden neurons outputs; grandmother cell, second from left). **e:** Example receptive fields for a network with $S > U$, relying on higher synergy between neurons to solve the task.

the collective interactions of recurrent neural circuits leading to cognitive function and behavior. Here, we show that PID opens a new window for assessing how specific computations arise from recurrent neural interactions. Unlike MI or TE, the PID quantifies the alternative ways in which a neuron determines the information in its output from its inputs, and thus can be a sensitive marker of different computational strategies. We here trained RNNs as models of cortical circuits [59] and used the PID to elucidate how the computations emerging from recurrent neural interactions contribute to task performance. We trained RNNs to solve a generalized version of the classic XOR classification problem with target labels corresponding to odd vs. even mixture components (Fig. 4a). Stimuli were presented for one time step ($t = 0$) and the network was trained to report the decision at $t = 10$. By tracking the temporal trajectories of the hidden layer activity we found that the network recurrent dynamics (represented as unfolded in time in Fig. 4b) progressively pulls the two input classes in opposite directions along the output weights (see Appendix). We used PID to dissect how a plurality of different strategies emerge from recurrent neural interactions in RNNs trained for solving a classification task. The computation emerged from the recurrent interaction between hidden neurons at different time steps. Do all successfully trained networks have a similar profile in terms of the PID terms? If so, this hints at a single computational strategy across these networks. If not, it is safe to assume that task performance is reached via different mechanisms, despite identical network architecture and training algorithm.

We found that on average across multiple networks S , R , and U rose with task difficulty (Fig. 4c), yet at all difficulties, individual networks differed strongly with respect to the ratio S/U , i.e. there were networks with larger average synergy across neuron pairs compared to the average unique information, and vice versa. For simple networks like the ones used here, one can inspect receptive fields to understand the reason for this differential behaviour (Fig. 4d-e). Indeed, networks with high average unique information displayed 'grandmother-cell'-like neurons, that would alone classify a large parts of the sample space, while in networks with higher average synergy such cells were absent (Fig. 4d). The emergence of these 'grandmother-cell'-like receptive fields is due to the recurrent dynamics. While in a feedforward architecture ($W_{XX} = 0$) hidden layer receptive fields are captured by hyperplanes in input space, in the RNN the receptive fields are time dependent, where later times are interpreted as deeper layers (Fig. 4b) and thus can capture highly non-linear features in input space. The advantage of PID versus a manual inspection of receptive fields is twofold: First, the PID framework abstracts and generalizes descriptions of receptive fields as being e.g. 'grandmother-cell'-like; thus the concept of unique information stays relevant even in scenarios where the concept of a receptive field becomes meaningless, or inaccessible. Second, the quantitative outcomes of a PID rest only on information theory, not specific assumptions about neural coding or computational strategies, and can be obtained for large numbers of neurons.

Comparison of our PID-based approach with the concept of neuronal selectivity used in neuroscience highlights interesting similarities and differences. Several kinds of selectivity (pure, mixed linear, and mixed non-linear) can be identified by performing regression analysis of neural responses vs. task variables [60]. In this framework, our grand-mother cells correspond to neurons with pure selectivity to the input class labels (a.k.a. "choice-selective" neurons). In the XOR task, [60] showed that non-linear mixed selectivity of neurons to the class labels is beneficial when solving the XOR task, by leading to a high-dimensional representation of the task variables. While selectivity profiles are a property of single neuron responses to task variables, our PID measures are a property of the combined activity of triplets of neurons and thus reveal emerging functional interactions between units and their computational algorithms (see also [7] and [52]). This allowed us to characterize a functional property of neural systems less studied than task variable selectivity: the computations that require functional mixing of the information from multiple units (measured by the average synergistic information) vs. the computations that rely on the output of individual neurons (measured by the unique information and described as grandmother cells). Concretely, by comparing PID and receptive fields we found that that in networks with high unique information, neurons typically have receptive fields with pure selectivity (grandmother cells, with large unique information to the class labels). In networks with high synergy, neurons show complex mixed selectivity to class labels.

5 Conclusions

We presented a partial information decomposition measure for continuous variables with arbitrary probability densities, thereby extending the popular BROJA PID measure for discrete variables. Extending PID measures to continuous variables drastically broadens the possible applications of the PID framework. This is important as the latter provides key insights into the way a complex system represents and modifies information in a computation – via asking which variables carry information about a target uniquely (such that it can only be obtained from that variable), redundantly, or only synergistically with other variables. Answering these questions is pivotal to understanding distributed computation in complex systems in general, and neural coding in particular. We believe that the methods presented here will allow PIDs to be extended efficiently in neuroscience for multiple continuous sources with potentially complex dependency structures, as would be common in cellular imaging data or activation properties of brain modules or areas in functional imaging. More generally, the approach we presented here would be relevant for other application domains such as machine learning, biomedical science, finance, and the physical sciences.

Acknowledgments

We thank Thibault Vatter and Praveen Venkatesh for conversations. The work of AP is supported by the Simons Foundation, the DARPA NESD program, NSF NeuroNex Award DBI1707398 and The Gatsby Charitable Foundation. DG is supported by a Swartz Fellowship. AM and MW are supported by Volkswagenstiftung under the program ‘Big Data in den Lebenswissenschaften’ and by the Ministry for Science and Education of Lower Saxony and the Volkswagen Foundation through the ‘Niedersächsisches Vorab’. LM is supported by NINDS Grant NS118461 (BRAIN Initiative). ES is supported by the Simons Collaboration on the Global Brain (542997) as well as research support from Martin Kushner Schnur and Mr. and Mrs. Lawrence Feis, and is the Joseph and Bessie Feinberg Professorial Chair.

References

- [1] Paul L Williams and Randall D Beer. Nonnegative decomposition of multivariate information. *arXiv preprint arXiv:1004.2515*, 2010.
- [2] Tycho Tax, Pedro AM Mediano, and Murray Shanahan. The partial information decomposition of generative neural network models. *Entropy*, 19(9):474, 2017.
- [3] Patricia Wollstadt, Sebastian Schmitt, and Michael Wibral. A rigorous information-theoretic definition of redundancy and relevancy in feature selection based on (partial) information decomposition. *arXiv preprint arXiv:2105.04187*, 2021.
- [4] Allison E Goodwell et al. Debates—does information theory provide a new paradigm for earth science? *Water Resources Research*, 56(2):e2019WR024940, 2020.
- [5] Benjamin Flecker, Wesley Alford, John M Beggs, Paul L Williams, and Randall D Beer. Partial information decomposition as a spatiotemporal filter. *Chaos*, 21(3):037104, 2011.
- [6] Michael Wibral, Joseph T Lizier, and Viola Priesemann. Bits from brains for biologically inspired computing. *Frontiers in Robotics and AI*, 2:5, 2015.
- [7] Nicholas M Timme, Shinya Ito, Maxym Myroshnychenko, Sunny Nigam, Masanori Shimono, Fang-Chin Yeh, Pawel Hottowy, Alan M Litke, and John M Beggs. High-degree neurons feed cortical computations. *PLoS computational biology*, 12(5):e1004858, 2016.
- [8] Michael Wibral, Viola Priesemann, Jim W Kay, Joseph T Lizier, and William A Phillips. Partial information decomposition as a unified approach to the specification of neural goal functions. *Brain and cognition*, 112:25–38, 2017.
- [9] Giuseppe Pica, Eugenio Piasini, Houman Safaai, Caroline Runyan, Christopher D Harvey, Mathew E Diamond, Christoph Kayser, Tommaso Fellin, and Stefano Panzeri. Quantifying how much sensory information in a neural code is relevant for behavior. In *NIPS*, 2017.
- [10] Jim W Kay, WA Phillips, Jaan Aru, Bruce P Graham, and Matthew E Larkum. A Bayesian decomposition of BAC firing as a mechanism for apical amplification in neocortical pyramidal neurons. *bioRxiv*, page 604066, 2019.
- [11] Itay Gat and Naftali Tishby. Synergy and redundancy among brain cells of behaving monkeys. In *Advances in neural information processing systems*, pages 111–117, 1999.
- [12] Naama Brenner, Steven P Strong, Roland Koberle, William Bialek, and Rob R de Ruyter van Steveninck. Synergy in a neural code. *Neural computation*, 12(7):1531–1552, 2000.
- [13] Elad Schneidman, William Bialek, and Michael J Berry. Synergy, redundancy, and independence in population codes. *Journal of Neuroscience*, 23(37), 2003.
- [14] Rodrigo Quian Quiroga and Stefano Panzeri. Extracting information from neuronal populations: information theory and decoding approaches. *Nature Reviews Neuroscience*, 10(3):173–185, 2009.
- [15] Nils Bertschinger, Johannes Rauh, Eckehard Olbrich, Jürgen Jost, and Nihat Ay. Quantifying unique information. *Entropy*, 16(4):2161–2183, 2014.
- [16] D Blackwell. Comparison of experiments. Proc. 2nd Berkeley Symp. Math. Stats. and Probability, 1951.

- [17] Moshe Leshno and Yishay Spector. An elementary proof of Blackwell’s theorem. *Mathematical Social Sciences*, 25(1):95–98, 1992.
- [18] Erik Torgersen. *Comparison of statistical experiments*. Cambridge University Press, 1991.
- [19] Lucien Le Cam. Comparison of experiments: A short review. *Lecture Notes-Monograph Series*, pages 127–138, 1996.
- [20] Nils Bertschinger, Johannes Rauh, Eckehard Olbrich, and Jürgen Jost. Shared information—new insights and problems in decomposing information in complex systems. In Thomas Gilbert, Markus Kirkilionis, and Gregoire Nicolis, editors, *Proceedings of the European Conference on Complex Systems 2012*, pages 251–269, Cham, 2013. Springer International Publishing.
- [21] Robin AA Ince. Measuring multivariate redundant information with pointwise common change in surprisal. *Entropy*, 19(7):318, 2017.
- [22] Conor Finn and Joseph T Lizier. Pointwise partial information decomposition using the specificity and ambiguity lattices. *Entropy*, 20(4):297, 2018.
- [23] Malte Harder, Christoph Salge, and Daniel Polani. Bivariate measure of redundant information. *Physical Review E*, 87(1):012130, 2013.
- [24] Johannes Rauh. Secret sharing and shared information. *Entropy*, 19(11):601, 2017.
- [25] Abdullah Makkeh, Aaron J Gutknecht, and Michael Wibral. Introducing a differentiable measure of pointwise shared information. *Physical Review E*, 103(3):032149, 2021.
- [26] Aaron J Gutknecht, Michael Wibral, and Abdullah Makkeh. Bits and pieces: Understanding information decomposition from part-whole relationships and formal logic. *Proceedings of the Royal Society A*, 477(2251):20210110, 2021.
- [27] Pradeep Kr Banerjee, Johannes Rauh, and Guido Montúfar. Computing the unique information. In *ISIT*, 2018.
- [28] Abdullah Makkeh, Dirk Oliver Theis, and Raul Vicente. Bivariate partial information decomposition: The optimization perspective. *Entropy*, 19(10):530, 2017.
- [29] Abdullah Makkeh, Dirk Oliver Theis, and Raul Vicente. Broja-2pid: A robust estimator for bivariate partial information decomposition. *Entropy*, 20(4):271, 2018.
- [30] Johannes Rauh, Maik Schünemann, and Jürgen Jost. Properties of unique information. *arXiv preprint arXiv:1912.12505*, 2019.
- [31] Adam B Barrett. Exploration of synergistic and redundant information sharing in static and dynamical Gaussian systems. *Physical Review E*, 91(5), 2015.
- [32] Gabriel Schamberg and Praveen Venkatesh. Partial Information Decomposition via Deficiency for Multivariate Gaussians. *arXiv preprint arXiv:2105.00769*, 2021.
- [33] M Sklar. Fonctions de repartition a n dimensions et leurs marges. *Publ. inst. statist. univ. Paris*, 8:229–231, 1959.
- [34] Harry Joe. *Multivariate Models and Multivariate Dependence Concepts*. CRC Press, May 1997.
- [35] Gal Elidan. Copulas in machine learning. In *Copulae in mathematical and quantitative finance*, pages 39–60. Springer, 2013.
- [36] Rafael S Calsaverini and Renato Vicente. An information-theoretic approach to statistical dependence: Copula information. *EPL (Europhysics Letters)*, 88(6):68003, 2009.
- [37] Jian Ma and Zengqi Sun. Mutual information is copula entropy. *Tsinghua Science & Technology*, 16(1):51–54, 2011.
- [38] Tim Bedford and Roger M Cooke. Probability density decomposition for conditionally dependent random variables modeled by vines. *Annals of Mathematics and Artificial intelligence*, 32(1-4):245–268, 2001.
- [39] Kjersti Aas, Claudia Czado, Arnoldo Frigessi, and Henrik Bakken. Pair-copula constructions of multiple dependence. *Insurance: Mathematics and economics*, 44(2):182–198, 2009.
- [40] Claudia Czado. Pair-copula constructions of multivariate copulas. In *Copula theory and its applications*, pages 93–109. Springer, 2010.

- [41] Thomas Nagler and Claudia Czado. Evading the curse of dimensionality in nonparametric density estimation with simplified vine copulas. *Journal of Multivariate Analysis*, 151:69–89, 2016.
- [42] Roger B Nelsen. *An Introduction to Copulas*. Springer Science & Business Media, June 2007.
- [43] Thomas Nagler and Thibault Vatter. `pyvinecopulib`, November 2020.
- [44] Yuri Burda, Roger Grosse, and Ruslan Salakhutdinov. Importance weighted autoencoders. *ICLR 2016*, 2016.
- [45] Diederik P Kingma and Max Welling. Auto-encoding variational bayes. *NIPS 2015*.
- [46] George Tucker, Dieterich Lawson, Shixiang Gu, and Chris J Maddison. Doubly reparameterized gradient estimators for Monte Carlo objectives. *ICLR*, 2019.
- [47] Diederik P Kingma and Jimmy Ba. Adam: A method for stochastic optimization. *ICLR 2015*.
- [48] Joseph T Lizier, Benjamin Flecker, and Paul L Williams. Towards a synergy-based approach to measuring information modification. In *2013 IEEE Symposium on Artificial Life (ALIFE)*, pages 43–51. IEEE, 2013.
- [49] Matteo Carandini and David J Heeger. Normalization as a canonical neural computation. *Nat. Rev. Neurosci.*, 13(1):51–62, November 2011.
- [50] Johannes Ballé, Valero Laparra, and Eero P Simoncelli. End-to-end optimized image compression. *ICLR*, 2017.
- [51] Andrew T Reid, Drew B Headley, Ravi D Mill, Ruben Sanchez-Romero, Lucina Q Uddin, Daniele Marinazzo, Daniel J Lurie, Pedro A Valdés-Sosa, Stephen José Hanson, Bharat B Biswal, et al. Advancing functional connectivity research from association to causation. *Nature neuroscience*, 22(11):1751–1760, 2019.
- [52] Michael Wibral, Conor Finn, Patricia Wollstadt, Joseph T Lizier, and Viola Priesemann. Quantifying information modification in developing neural networks via partial information decomposition. *Entropy*, 19(9):494, 2017.
- [53] Thomas Schreiber. Measuring information transfer. *Physical review letters*, 85(2):461, 2000.
- [54] Raul Vicente, Michael Wibral, Michael Lindner, and Gordon Pipa. Transfer entropy—a model-free measure of effective connectivity for the neurosciences. *Journal of computational neuroscience*, 30(1):45–67, 2011.
- [55] Leonardo Novelli and Joseph T Lizier. Inferring network properties from time series using transfer entropy and mutual information: validation of multivariate versus bivariate approaches. *Network Neuroscience*, 5(2):373–404, 2021.
- [56] Paul L Williams and Randall D Beer. Generalized measures of information transfer. *arXiv preprint arXiv:1102.1507*, 2011.
- [57] Amin Nejatbakhsh, Francesco Fumarola, Saleh Esteki, Taro Toyozumi, Roozbeh Kiani, and Luca Mazzucato. Predicting perturbation effects from resting state activity using functional causal flow. *bioRxiv*, 2020.
- [58] Patricia Wollstadt, Joseph T Lizier, Raul Vicente, Conor Finn, Mario Martinez-Zarzuela, Pedro Mediano, Leonardo Novelli, and Michael Wibral. `idtxl`: The information dynamics toolkit xl: a python package for the efficient analysis of multivariate information dynamics in networks. *Journal of Open Source Software*, 4(34):1081, 2019.
- [59] Valerio Mante, David Sussillo, Krishna V Shenoy, and William T Newsome. Context-dependent computation by recurrent dynamics in prefrontal cortex. *nature*, 503(7474):78–84, 2013.
- [60] Mattia Rigotti, Omri Barak, Melissa R Warden, Xiao-Jing Wang, Nathaniel D Daw, Earl K Miller, and Stefano Fusi. The importance of mixed selectivity in complex cognitive tasks. *Nature*, 497(7451):585–590, 2013.
- [61] Tom Rainforth, Adam Kosiorek, Tuan Anh Le, Chris Maddison, Maximilian Igl, Frank Wood, and Yee Whye Teh. Tighter variational bounds are not necessarily better. In *ICML*, 2018.
- [62] Murray Rosenblatt. Remarks on a multivariate transformation. *The annals of mathematical statistics*, 23(3):470–472, 1952.

Supplementary Material

A Estimating the gradients

As shown in Section 3, the unique information $U(Y : X_1 \setminus X_2)$ is upper bounded as

$$I_q[\theta] \leq B_1[\theta] + B_2[\theta, \phi], \quad (\text{A.1})$$

where

$$B_1[\theta] = \mathbb{E}_{c_\theta(u_y, u_1, u_2)} \log [c(u_y, u_1) c_{1,2|\theta(u_y)}(u_{1|y}, u_{2|y})], \quad (\text{A.2})$$

$$B_2[\theta, \phi] = -\mathbb{E}_{c_\theta(u_1, u_2)} D_{A,\theta,\phi}(u_1, u_2), \quad (\text{A.3})$$

and

$$D_{A,\theta,\phi}(u_1, u_2) = \mathbb{E}_{r_\phi(u_y^{(1)} \dots u_y^{(A)} | u_1, u_2)} \log \left[\frac{1}{A} \sum_{a=1}^A \frac{c_\theta(u_y^{(a)}, u_1, u_2)}{r_\phi(u_y^{(a)} | u_1, u_2)} \right], \quad (\text{A.4})$$

and the above expectation is w.r.t.

$$r_\phi(u_y^{(1)} \dots u_y^{(A)} | u_1, u_2) \equiv \prod_{a=1}^A r_\phi(u_y^{(a)} | u_1, u_2). \quad (\text{A.5})$$

The parametrization we use for the inference distribution $r_\phi(u_y | u_1, u_2)$ is detailed below in Appendix D. We are interested in minimizing the r.h.s. of (A.1) w.r.t. (θ, ϕ) . To obtain low-variance gradients, it is convenient to eliminate the θ, ϕ dependence in the measures of (A.2)-(A.4) using the ‘reparametrization trick’ [45].

The idea is to obtain samples from $c_\theta(u_y, u_1, u_2)$ by a θ -dependent transformation of three $\text{Unif}[0, 1]$ samples $\mathbf{v} = (v_y, v_1, v_2)$, and samples from $r_\phi(u_y | u_1, u_2)$ by a (u_1, u_2, ϕ) -dependent transformation of $\epsilon \sim \text{Unif}[0, 1]$. We present the details of these transformations in Appendices C and D, respectively.

Taking M samples of $c_\theta(u_y, u_1, u_2)$ and denoting them as $\bar{u}_y^{(m)}, \bar{u}_1^{(m)}, \bar{u}_2^{(m)}$, we can estimate (A.2) as

$$B_1[\theta] \simeq \frac{1}{M} \sum_{m=1}^M \log \left[c(\bar{u}_y^{(m)}, \bar{u}_1^{(m)}) c_{1,2|\theta(\bar{u}_y^{(m)})}(\bar{u}_{1|y}^{(m)}, \bar{u}_{2|y}^{(m)}) \right] \quad (\text{A.6})$$

where we denoted $\bar{u}_{i|y} = F(u_i = \bar{u}_i | u_y = \bar{u}_y)$ for $i = 1, 2$. An estimate of the gradient $\nabla_\theta B_1$ is obtained by acting on this expression with ∇_θ , which also acts on the θ -dependent samples.

Denoting A samples from $r_\phi(u_y | u_1, u_2)$ as $\hat{u}_y^{(a)}$, we can also estimate (A.3) as

$$B_2[\theta, \phi] \simeq -\frac{1}{M} \sum_{m=1}^M \log \left(\frac{1}{K} \sum_{a=1}^A w_{a,m} \right), \quad (\text{A.7})$$

where we defined

$$w_{a,m} = \frac{c_\theta(\hat{u}_y^{(a)}, \bar{u}_1^{(m)}, \bar{u}_2^{(m)})}{r_\phi(\hat{u}_y^{(a)} | \bar{u}_1^{(m)}, \bar{u}_2^{(m)})}. \quad (\text{A.8})$$

Acting on this expressions with ∇_θ yields an estimate of $\nabla_\theta B_2$. On the other hand, as noted in [61], the estimate of $\nabla_\phi B_2$ resulting from acting with ∇_ϕ on (A.7) has a signal-to-noise ratio which decreases with A . A solution to this problem was found in [46], which showed that a stable gradient estimate can be obtained instead as

$$\nabla_\phi B_2 \simeq \frac{-1}{M} \sum_{m=1}^M \sum_{a=1}^A \left(\frac{w_{a,m}}{\sum_{s=1}^A w_{s,m}} \right)^2 \frac{\partial \log w_{a,m}}{\partial \hat{u}_y^{(a)}} \nabla_\phi \hat{u}_y^{(a)}, \quad (\text{A.9})$$

and this is the estimate we use in our experiments.

B The bivariate Gaussian copula

A bivariate Gaussian copula is parametrized by $\theta \in [-1, 1]$ and given by

$$c(u_1, u_2) = \frac{1}{\sqrt{1-\theta^2}} \exp \left\{ -\frac{\theta^2(x_1^2 + x_2^2) - 2\theta x_1 x_2}{2(1-\theta^2)} \right\} \quad (\text{B.1})$$

where $x_i = \Phi^{-1}(u_i)$ and Φ is the standard univariate Gaussian CDF. For explicit expressions of other popular bivariate copulas, see [39].

C Sampling from the copula

In this section we show how to obtain samples from the three-dimensional copula

$$c_\theta(u_y, u_1, u_2) = c(u_y, u_1) c(u_y, u_2) c_{1,2|y,\theta}(u_{1|y}, u_{2|y}) \quad (\text{C.1})$$

by applying a θ -dependent transformation to samples from $\text{Unif}[0, 1]$. We use the Rosenblatt transform [62], which consists in using the inverse CDF method to sample from each factor in

$$c(u_y, u_1, u_2) = c(u_1) c(u_y|u_1) c(u_2|u_y, u_1). \quad (\text{C.2})$$

We denote $F(\cdot|\cdot)$ is the CDF of $c(\cdot|\cdot)$. Adopting the notation of [39], we define

$$h_{ij}(u_i, u_j) = F(u_i|u_j) = \frac{\partial C(u_i, u_j)}{\partial u_j} \quad i, j = 1, 2. \quad (\text{C.3})$$

For several popular parametric families of bivariate copulas, such as those we consider in this paper, explicit expressions are known for $h_{ij}(u_i, u_j)$ along with its inverse $h_{ij}^{-1}(\cdot, u_j)$ w.r.t. the first argument (see e.g. [39]). Note that using this notation, the arguments in the last factor of (C.1) are $u_{i|y} = h_{iy}(u_i, u_y)$ ($i=1,2$).

We first sample (v_1, v_y, v_2) from $\text{Unif}[0, 1]$ and successively obtain u_1, u_y, u_2 by inverting the functions in the r.h.s. of

$$\begin{aligned} v_1 &= F(u_1), \\ &= u_1, \\ v_y &= F(u_y|u_1), \\ &= h_{y1}(u_y, u_1), \\ v_2 &= F(u_2|u_1, u_y), \\ &= h_{21|\theta(u_y)}(F(u_2|u_y), F(u_1|u_y)), \\ &= h_{21|\theta(u_y)}(h_{2y}(u_2, u_y), h_{1y}(u_1, u_y)). \end{aligned}$$

Explicitly, we get

$$\begin{aligned} u_1 &= v_1, \\ u_y &= h_{y1}^{-1}(v_y, u_1), \\ u_2 &= h_{2y}^{-1}(h_{21|\theta(u_y)}^{-1}(v_2, h_{y1}(u_y, u_1)), u_y). \end{aligned}$$

Note that only u_2 actually depends on θ .

D Parametrization of the learned models

D.1 Parametrizing the learned conditional copula

The conditional Gaussian copula $c_{1,2|\theta(u_y)}(u_{1|y}, u_{2|y})$ is parametrized by the function $\theta(u_y): [0, 1] \rightarrow [-1, +1]$. For its functional form we used

$$\theta(u_y) = \tanh \left(\sum_{i=1}^{16} w_{2,i} \tanh(w_{1,i} u_y + b_1) + b_2 \right) \quad (\text{D.1})$$

where $w_{1,i}, w_{2,i}, b_1, b_2 \in \mathbb{R}$.

D.2 Parametrizing and sampling from the inference distribution

In our experiments we parametrize the inference distribution $r_\phi(u_y|u_1, u_2)$ via its CDF, as

$$\begin{aligned} R_\phi(u_y|u_1, u_2) &= \int_0^{u_y} du r_\phi(u|u_1, u_2), \\ &= \frac{1}{1 + e^{-z(u_y)a_\phi(u_1, u_2) - b_\phi(u_1, u_2)}}, \end{aligned} \quad (\text{D.2})$$

where $z(u_y) = \log \left(\frac{u_y}{1-u_y} \right)$. Derivating w.r.t. u_y gives

$$r_\phi(u_y|u_1, u_2) = R_\phi(1 - R_\phi)a_\phi(u_y^{-1} + (1 - u_y)^{-1}). \quad (\text{D.3})$$

The functions $a_\phi(u_1, u_2)$ and $b_\phi(u_1, u_2)$ take values in \mathbb{R} and are parametrized with a neural network with two hidden layers, and we impose $a_\phi(u_1, u_2) > 0$ in order to make R_ϕ monotonous with u_y . In order to sample from r_ϕ , we draw $\epsilon \sim \text{Unif}[0, 1]$, and use the inverse CDF method to obtain

$$\begin{aligned} u_y(\epsilon, u_1, u_2) &= R_\phi^{-1}(\epsilon|u_1, u_2), \\ &= \frac{1}{1 + e^{-(z(\epsilon) - b_\phi(u_1, u_2))/a_\phi(u_1, u_2)}}. \end{aligned} \quad (\text{D.4})$$

E Comparison with a discrete estimator

In this section we estimate the PID of the two models of three neurons from eq. (4.2) using the discrete estimator BROJA-2PID [29]. In particular, we present a quantization scheme of the continuous models that leads to a qualitative agreement between the discrete and continuous estimators, thus further validating the results of the latter.

Let us denote the discretized versions of X_1, X_2, Y as $\hat{x}_1, \hat{x}_2, \hat{y}$. The discrete PID estimators require as input a distribution $p(\hat{x}_1, \hat{x}_2, \hat{y})$ [29]. To create the latter from our continuous models in eq. (4.2), we start by dividing the continuous range of each $X_i (i = 1, 2)$ into N_x segments, and associate each segment with a discrete value \hat{x}_i equal to the value of X_i in the middle of each segment. To each square in the resulting 2D $N_x \times N_x$ grid we associate a discrete probability $p(\hat{x}_1, \hat{x}_2)$ equal to the integral of the joint Gaussian density of (X_1, X_2) in the square. Finally, in each of the two models, we split the Y range into N_y segments $\{s_i\}_{i=1}^{N_y}$. The boundaries of the segments are chosen such that the same fraction $1/N_y$ of values of $Y = Y(X_1, X_2)$ falls into each segment using eq. (4.2), a procedure called ‘maximum entropy binning’. Let $\hat{y} \in \{1 \dots N_y\}$. Using this quantization, the three-dimensional discrete distribution is defined as

$$p(\hat{x}_1, \hat{x}_2, \hat{y}) = \begin{cases} p(\hat{x}_1, \hat{x}_2) & \text{if } Y(\hat{x}_1, \hat{x}_2) \in s_{\hat{y}}, \\ 0 & \text{if } Y(\hat{x}_1, \hat{x}_2) \notin s_{\hat{y}}, \end{cases} \quad (\text{E.1})$$

where in each model $Y(\hat{x}_1, \hat{x}_2)$ is obtained from eq. (4.2). Fig. 5 shows the results of the discrete PID obtained using this quantization for the two models considered, assuming $X_i \in [-8, 8]$ and $N_x = 16$ equally-sized segments. For the Y quantization we used $N_y = 3$. Note the qualitative agreement with the continuous results in Fig. 2.

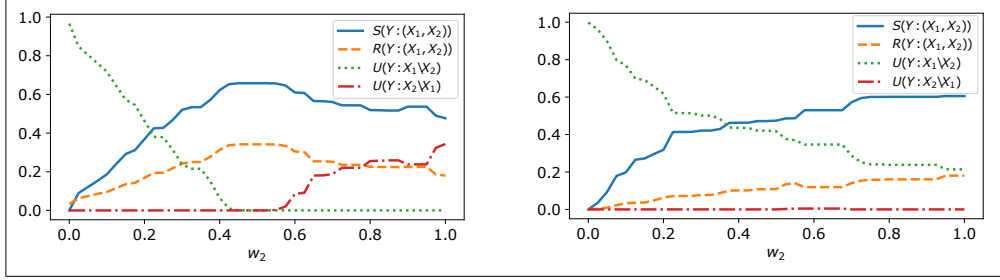


Figure 5: **Qualitative agreement of discrete and continuous PID estimations.** The two models are defined in (4.2) (left: Model 1, right: Model 2), and we used the same model parameters indicated in Fig. 2. We show the normalized discrete PID terms as a function of the synaptic strength w_2 . See the text for details on the discrete quantization used. Note that for both models the discrete results agree qualitatively with the continuous results in Fig. 2.

F Consistency

Using Model 2 from Eq.(4.2) as an example, we compared estimates of $U(Y : X_2 \setminus X_1)$ with indirect estimates obtained from applying the consistency conditions to estimates of $U(Y : X_1 \setminus X_2)$. The results in Figure 6 show good agreement, thus further validating the method.

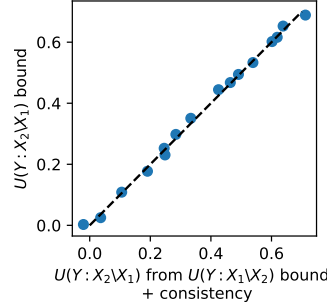


Figure 6: Comparison of direct vs. indirect estimates of $U(Y : X_2 \setminus X_1)$, illustrating the consistency of the method.

G More on the experiments

In this section we provide more details on the last two experiments presented in Section 4.

Computational aspects of connectivity in recurrent neural circuits.

We start by deriving the relation $TE = S + U_1$ verified in this experiment (Fig. 3d). Transfer entropy [53] $TE(X \rightarrow Y)$ is defined as $I(Y^+ : X^- | Y^-)$ where Y^+ is the future of state of Y , X^- and Y^- are the past states of X and Y , respectively. Consider the chain rule for mutual information,

$$I(Y^+ : (X^-, Y^-)) = I(Y^+ : Y^-) + I(Y^+ : X^- | Y^-). \quad (\text{G.1})$$

Replacing $I(Y^+ : (X^-, Y^-))$ and $I(Y^+ : Y^-)$ by the r.h.s. of (1.1) and (1.3), we get

$$I(Y^+ : X^- | Y^-) = U(Y^+ : X^- \setminus Y^-) + S(Y^+ : (X^-, Y^-)), \quad (\text{G.2})$$

N	K=4				K=6				K=8				K=10			
	UI	SI	MI	W	UI	SI	MI	W	UI	SI	MI	W	UI	SI	MI	W
1	0.28	0.27	1.22	-0.05	0.72	0.38	1.1	-0.11	0	0.22	1.59	0.09	0.05	0.19	2.7	0.27
2	0.39	0.59	0.9	-0.57	0.01	0.39	1.24	-0.15	1.58	0.42	2.93	-0.57	1.74	0.13	3.47	-0.55
3	0.04	0.39	0.84	0.18	0.01	0.39	0.93	-0.14	0.04	0.05	1.18	0.07	0.38	0.46	2.21	0.04
4	0.01	0.22	1.2	-0.38	0.02	0.32	0.93	0.02	0.34	0.33	2.16	0.03	0	0.37	1.24	0.02
5	0.4	0.29	1.38	-0.34	0.56	0.69	1.8	-0.43	0.01	0.41	3.39	-0.62	0.02	0.2	2.32	-0.21

Table 1: **Node-specific details for generalized XOR task:** Average node-specific unique, synergistic, and mutual information (UI, SI, MI) and the decoding weight for different nodes in the hidden layer ($N \in \{1, \dots, 5\}$) and for different task difficulty levels ($K \in \{4, 6, 8, 10\}$).

which is the equation we verified by estimating separately the left and right sides. The two terms in the r.h.s. are called *state-independent transfer entropy* and *state-dependent transfer entropy* respectively in [56], reflecting their intuitive meaning.

In Fig. 7, we analyze the state space of the network in Fig. 3 of the main text. The activities of the upstream sub-network X and downstream sub-network Y are shown, projected onto their first two principal components (PCs). The causal structure and algorithmic details of the effective connectivity between the two sub-networks cannot be identified solely by the observation of their geometrical properties.

Uncovering a plurality of computational strategies in RNNs trained to solve complex tasks.

Each RNN has fully connected architecture with \tanh non-linearity. Data was generated by sampling from the GMM with K components ($K \in \{4, 6, 8, 10\}$) in batches of 128 data points with the total number of 3000 batches. The RNNs were trained using standard backprop in time using Adam optimizer in Pytorch package with a learning rate of 0.01. For each trained RNN we considered all triplets (Y, X_i, X_j) where $i, j \in \{1, \dots, 5\}$, i.e. the target variable is the output of the network Y and the source variables iterate over all pairs of the hidden nodes in the RNN. Once the RNN is trained we collect a test sample of 1000 data points from the same GMM used for training, and evaluate the nodes when inputting the RNN using test data and running it forward for $t = 10$ time steps. This gives us 1000 samples from each variable $X_{1:5}, Y$ which we then use for PID analysis on the triplets mentioned above. For each level of task difficulty $K \in \{4, 6, 8, 10\}$ we trained 5 RNNs and performed PID ($A = 100$) on the resulting trained networks.

In Fig. 8 more details on the trained RNN's in Fig. 4 of the main text are illustrated, providing more insight into the computational strategies employed by each trained instance as the task complexity grows. The first row shows the time evolution of the recurrent layer of hidden units projected onto their first 3 PC's. For these RNN instances, the ones with $K = 6, 10$ have grand mother-like cells (as confirmed by the receptive field plots in Fig. 8c), with large unique information compared to the other cells. These grand mother-like cells cannot be inferred by just inspecting the geometry of the hidden units in the state space, but can be identified with the PID. PID reveals more details about the computation and the differences between strategies for different instances of trained RNN's. Details of the PID for individual hidden nodes including average unique and synergistic information for each node, its mutual information with the output node, and the decoding weight connecting the hidden node to the output unit is included in Table 1.

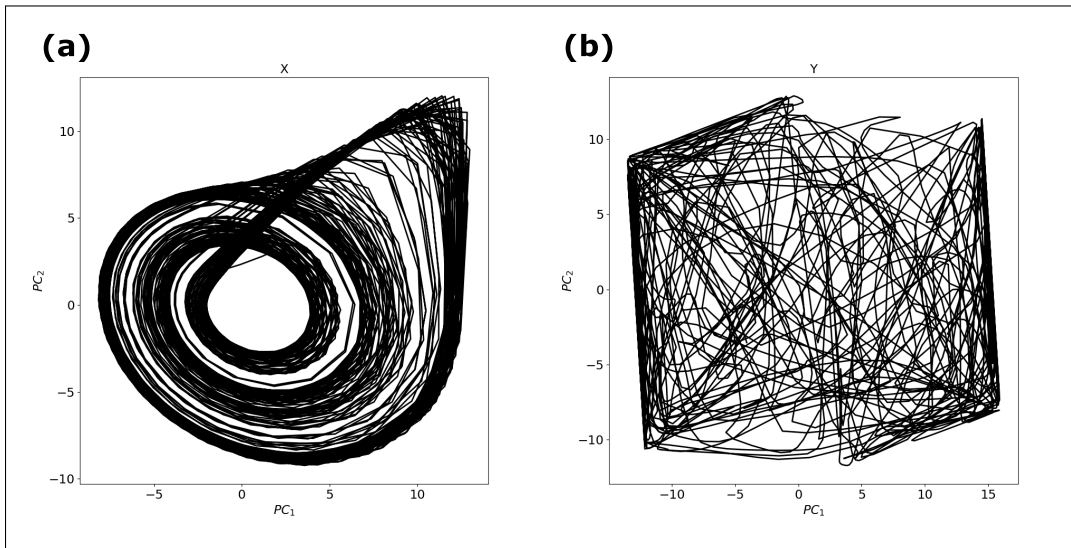


Figure 7: **State space of the chaotic network of rate neurons:** Projection of the state space of the recurrent units for upstream network X (a) and downstream network Y (b) onto their respective first two principal components.

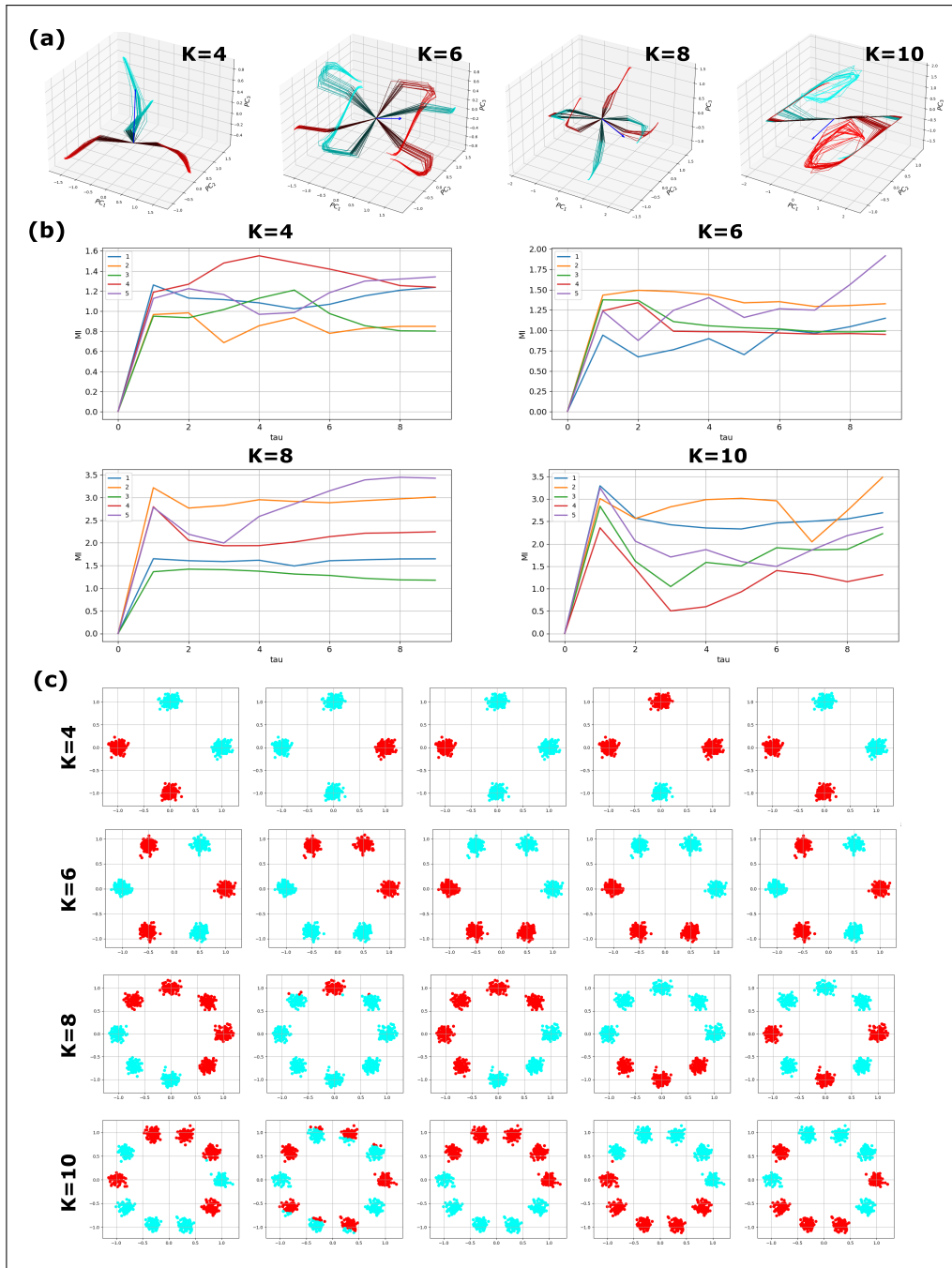


Figure 8: **Algorithmic investigation of trained RNNs on generalized XOR task:** (a) Evolution of the hidden unit activations in time (recurrent time steps). Darker colors correspond to earlier time points; red and cyan correspond to even and odd trials. Blue arrow corresponds to decoding direction, i.e. the predicted label is given by the sign of the projection of the last time point of each trajectory onto this direction. (b) Mutual information between individual hidden units and the output of the network as a function of recurrent time steps for the different tasks. (c) Receptive fields of individual neurons, in certain cases ($K=6$, unit 1 and $K=10$, unit 2) grand mother-like cells can be observed, yielding greater unique information than synergistic information hinting at the algorithmic strategy employed by that instance of the trained RNN.